Available online at www.sciencedirect.com
ScienceDirect
International Journal of Heat and Mass Transfer 51 (2008) 2863–2870
International Journal of HEAT and MASS TRANSFER
www.elsevier.com/locate/ijhmt

Field synergy analysis and optimization of the convective mass transfer in photocatalytic oxidation reactors

Qun Chen, Ji-an Meng *

Department of Engineering Mechanics, Tsinghua University, Beijing 100084, PR China

Received 29 April 2007; received in revised form 11 September 2007
Available online 5 November 2007

Abstract

A convective mass transfer field synergy equation with a specific boundary condition for photocatalytic oxidation reactors developed based on the extremum principle of mass transfer potential capacity dissipation can be used to increase the field synergy between the velocity and contaminant concentration gradient fields over the entire fluid flow domain to enhance the convective mass transfer and increase the contaminant removal effectiveness of photocatalytic oxidation reactors. The solution of the field synergy equation gives the optimal flow field, having the best field synergy for a given viscous dissipation, which maximize the contaminant removal effectiveness. As an illustrative example, the field synergy analysis for laminar mass transfer in plate type reactors is presented. The analysis shows that generating multiple longitudinal vortex flow in the plate type reactor effectively enhances the laminar mass transfer. With the guide of the optimal velocity pattern, the discrete double-inclined ribs can be introduced in actual applications to generate the desired multi-longitudinal vortex flow, so as to enhance the laminar mass transfer, and consequently, improve the contaminant removal performance. The experimental result shows that the contaminant removal effectiveness for the discrete double-inclined ribs plate reactor is increased by 22% compared to the smooth plate reactor.

Keywords: Convective mass transfer; Field synergy equation; Mass transfer potential capacity dissipation; Photocatalytic oxidation reactors; Optimization

1. Introduction

Indoor air quality, which is mostly a function of the contaminant concentration, is very important to people's health and comfort [1–3]. In recent era of energy shortages, buildings have been sealed tightly and fresh air flow rate in air conditioning systems has been decreased sharply to reduce energy consumption. Meanwhile, volatile ornamental materials, household appliances and office equipment (e.g. computers, televisions and printers) that emit volatile organic compounds (VOCs) have become much more widely used. These factors have resulted in increased indoor contaminant concentrations, which are often associated with adverse healthy effects including headache, dry cough and nausea. Therefore, it has fueled huge interest in new effective approaches to reduce VOC concentration.

Photocatalytic oxidation (PCO) by employing ultraviolet (UV) radiation, which offers several environmental and practical advantages over conventional biological or physical disinfection processes include eliminating the contaminant sources and diluting the contaminant concentration with fresh air, is an innovative and promising technology to remove VOCs [4–11]. However, a commercial competitive full-scale photocatalytic oxidation system has not yet been widely accepted in practice. One of the major barriers is its low energy efficiency due, among other factors, to the limited capacity to deliver reactants to catalyst surfaces [12]. And it is found that for many cases, the mass transfer ability of the PCO reactors are the bottleneck factors of improving their VOC removal effectiveness [13].

* Corresponding author. Tel.: +86 10 62773776; fax: +86 10 62781610.
E-mail address: mja@tsinghua.edu.cn (J.-a. Meng).

0017-9310/$ - see front matter © 2007 Elsevier Ltd. All rights reserved.
doi:10.1016/j.ijheatmasstransfer.2007.09.024

Nomenclature

C	contaminant concentration, kg m^{-3}
D	mass diffusion coefficient, m^2 s^{-1}
F	additional volume force per unit volume, N m^{-3}
Fs	field synergy number
J^*	Lagrange function
K	Langmuir adsorption equilibrium constant, m^3 mg^{-1}
k	reaction constant, mol m^{-2} s^{-1}
$\vec{n}$	outward normal unit vector
P	pressure, Pa
r	photocatalytic reaction rate, mol m^{-2} s^{-1}
Re	Reynolds number
S	surface area, m^2
Sc	Schmidt number
Sh	Sherwood number
u, v, w	velocity component in x-, y- and z-directions, m s^{-1}
$\vec{U}$	velocity vector
V	volume, m^3
x, y, z	Cartesian coordinates, m
Y	mass fraction
Z_m	mass transfer potential capacity dissipation function, kg s^{-1} m^{-3}
ε	contaminant removal effectiveness
ρ	air density, kg m^{-3}
μ	dynamic viscosity, kg m^{-1} s^{-1}
Φ	viscous dissipation function, W m^{-3}
∇	divergence operator
Ω	flow domain
Γ	flow domain boundary
A, C_1, C_Φ, E_1, E_2, F_1	Lagrange multiplier

Subscripts

c	constant
s	catalyst surface
in	inlet
out	outlet

In the last several decades of the twentieth century, a large number of novel geometry of the PCO reactors had been developed including plate type reactors, corrugated plate reactors [14], light-in-tube reactor, and honeycomb type reactors [15], to improve the capacity of delivering contaminants. However, most techniques were developed empirically or semi-empirically.

Guo et al. [16] introduced the field synergy concept to improve convective heat transfer performance based on the synergy between the velocity and temperature gradient fields in the fluid flow domain, and then developed the field synergy principle, which states that the overall heat transfer rate depends not only on the velocity and the temperature gradient field, but also on their synergy. For a given set of constraints, an optimal velocity field exists, which improves the synergy between the velocity and temperature gradient fields to maximize the heat transfer rate. This principle has been validated numerically and experimentally [17,18]. Furthermore, Meng et al. [18] then deduced the laminar heat transfer field synergy equation based on the extremum entransy dissipation principle [19], which was originally referred to as the heat transfer potential capacity dissipation extremum principle. The solution of the laminar field synergy equation gave the optimal velocity field, which has a significantly larger heat transfer rate for a given pumping power, for optimizing heat transfer processes.

Delivering reactants to catalyst surfaces is a convective mass transfer process essentially, which is analog to a convective heat transfer process. Mo et al. [13] used the field synergy concept to analyses the influence of the included angle between the velocity and the contaminant concentration gradient vectors to the convective mass transfer rate in the reactor. Chen et al. [20] introduced the convective mass transfer field synergy principle, which states that the overall mass transfer rate depends not only on the velocity and concentration gradient fields, but also on their synergy. Furthermore, Chen et al. [20] also deduced the laminar mass transfer field synergy equation and found a universal method for optimizing indoor decontamination ventilation designs. However, the boundary conditions of photocatalytic oxidation reactors are different from the ones of indoor contaminant sources, and the universal method for optimizing the mass transfer process in photocatalytic oxidation reactors has not been obtained.

This paper first deduces a mass transfer field synergy equation with a specific boundary condition for optimizing the processes of delivering reactants to catalyst surfaces in photocatalytic oxidation reactors. Then the optimal velocity field, which has a large mass transfer rate for a given pumping power, can be obtained by solving the field synergy equation to provide a framework for guiding the photocatalytic oxidation reactors designs. Finally, as an illustrative example, the field synergy analysis is used to optimize the convective mass transfer in plate type reactors to verify the applicability of the convective mass transfer field synergy equation.

2. Theoretical model of photocatalytic oxidation reactors

There are several types of PCO reactors such as plate type reactors, light-in-tube reactors, and honeycomb type reactors. The theoretical schematic of these reactors are summarized in Fig. 1. The upper surface is a UV lamp, which emits ultraviolet photos. The lower is a catalyst surface coated with semiconductor materials such as titanium dioxide (TiO_2). When semiconductor materials are illumi-

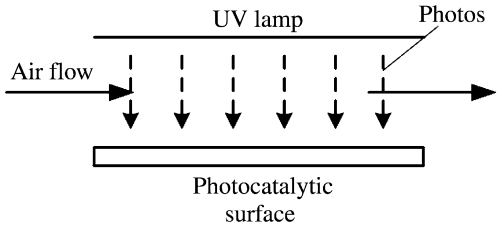

Fig. 1. Schematic of a generalized PCO reactor.

nated by photons, the electrons in the valence band of the material are excited into the conduction band which leaves electron holes in the valence band. The components of this activated pair are capable of oxidizing a surface-absorbed organic compound being from the air. When air flows in the channel, the organic compounds in the air transfer to the catalyst surface on account of the concentration gradient, and then adsorbed by the activated electrons and holes. The surface-absorbed organic compounds are catalyzed on the catalyst surface. Finally, the reaction products are desorbed from the catalyst surface and transfer into the air.

For simplicity, the follow assumptions are made: (1) the photocatalytic reaction is a first-order reaction with a constant reaction coefficient; (2) the absorption and desorption processes are quick enough; (3) there is only one species of VOCs in the air; (4) the density of the air is constant; (5) the reaction product has no influence on the reaction process. For these assumptions, the steady-state photocatalytic oxidation is described by the following equation:

Mass continuity equation:

$$\nabla \cdot \rho \vec{U} = 0, \tag{1}$$

where ρ is the density of the air and $\vec{U}$ is the velocity vector of the air.

Momentum equation:

$$\rho \vec{U} \cdot \nabla \vec{U} = -\nabla P + \nabla \cdot (\mu \nabla \vec{U}) + \vec{F}, \tag{2}$$

where P is the pressure and μ is the dynamic viscosity.

Species equation:

$$\rho \vec{U} \cdot \nabla Y = \nabla \cdot (\rho D \nabla Y), \tag{3}$$

where Y is the mass fraction of the species and D is the mass diffusion coefficient.

Boundary conditions on the catalyst surface:

$$r = k \frac{KC_s}{1 + KC_s}, \tag{4}$$

where r is the photocatalytic reaction rate, k is the reaction constant, K is the Langmuir adsorption equilibrium constant, C_s is the contaminant concentration in the air nearby the reaction surface.

The contaminant removal effectiveness of a PCO reactor can be characterized by the fractional conversion of a PCO reactor

$$\varepsilon = \frac{C_{in} - C_{out}}{C_{in}}, \tag{5}$$

where C_{in} is the contaminant concentration at the air inlet, C_{out} is the contaminant concentration at the outlet.

3. Field synergy principle and field synergy equation for convective mass transfer processes in photocatalytic oxidation reactors

Chen et al. [20] integrated the Species equation for laminar flow over the entire flow domain while neglecting the axial mass diffusion at the fluid inlets and outlets to get:

$$\int_{\Omega} \rho \vec{U} \cdot \nabla Y \, dV = \int_{Wall} \vec{n} \cdot (\rho D \nabla Y) \, dS. \tag{6}$$

The dimensionless form of Eq. (6) is

$$Sh = ReSc \int_{\Omega} \overline{\vec{U}} \cdot \nabla \overline{Y} \, d\overline{V}, \tag{7}$$

where Sh, Re and Sc represent the Sherwood number, the Reynolds number and the Schmidt number, respectively. Eq. (7) shows that the Sherwood number depends not only on the Reynolds number and the Schmidt number but also on the value of $\int_{\Omega} \overline{\vec{U}} \cdot \nabla \overline{Y} \, d\overline{V}$, which is defined as the mass transfer field synergy number,

$$FS_m = \int_{\Omega} \overline{\vec{U}} \cdot \nabla \overline{Y} \, d\overline{V} = \int_{\Omega} |\overline{\vec{U}}||\nabla \overline{Y}| \cos\beta \, d\overline{V}, \tag{8}$$

where β is the included angle between the velocity and mass concentration gradient vectors. FS_m, depends not only on the velocity and the concentration gradient, but also on their included angle (their synergy). A smaller included angle between the two vectors leads to a larger field synergy number for the velocity and concentration gradient fields in the fluid domain.

Transforming Eq. (7) into another form gives:

$$\frac{Sh}{ReSc} = FS_m. \tag{9}$$

For given Re number and Sc number, a larger field synergy number leads to a higher boundary mass flux then referred to as a higher photocatalytic reaction rate. Therefore, the optimal velocity and contaminant concentration fields, which have a larger field synergy number, will enhance the convective mass heat transfer in photocatalytic oxidation reactors.

Mass transfer is an irreversible process. When species is transported from higher concentration fields to lower concentration fields, the mass is conserved, but the mass transfer capacity is not conserved due to its dissipation by the mass transfer resistance. This dissipation is defined as the mass transfer potential capacity dissipation, $Z_m = \rho D \nabla Y \cdot \nabla Y$ [20].

For photocatalytic oxidation reactors, enhancing reaction rate means maximizing the mass flux, which leads to the maximum of mass transfer potential capacity dissipation. Therefore, the optimization objective is to find an

optimal velocity field, which has the maximum of the mass transfer potential capacity dissipation, for some specified constraints including the mass continuity equation, species equation, constant viscous dissipations, as well as the boundary conditions on the catalyst surface. This is a typical variational extremum problem in mathematics. These constraints can be removed by using the Lagrange multipliers method to construct a function [21,22]

$$J^* = \int\int\int_{\Omega}[\rho D\nabla Y\cdot\nabla Y + C_{\Phi}\Phi + A(\rho D\nabla\cdot\nabla Y - \rho\vec{U}\cdot\nabla Y) + C_1\nabla\cdot\rho\vec{U}]\,\mathrm{d}V + \int\int_{\Gamma_s}E_1\vec{U}\,\mathrm{d}S + \int\int_{\Gamma_u}E_2(\vec{U}-\vec{U}_c)\,\mathrm{d}S + \int\int_{\Gamma_r}F_1\left(-\vec{n}\cdot\frac{(1+K\rho Y)D\nabla Y}{Y} - (kK)_c\right)\mathrm{d}S, \quad (10)$$

where A, C_1, C_{Φ}, E_1, E_2 and F_1 are Lagrange multiplies. A, C_1, E_1, E_2 and F_1 vary with position, while C_{Φ} is constant for a given viscous dissipation. Φ is the viscous dissipation function, which is expressed as

$$\Phi = \mu\begin{bmatrix} 2\left(\frac{\partial u}{\partial x}\right)^2 + 2\left(\frac{\partial v}{\partial y}\right)^2 + 2\left(\frac{\partial w}{\partial z}\right)^2 \\ +\left(\frac{\partial u}{\partial y}+\frac{\partial v}{\partial x}\right)^2 + \left(\frac{\partial u}{\partial z}+\frac{\partial w}{\partial x}\right)^2 + \left(\frac{\partial v}{\partial z}+\frac{\partial w}{\partial y}\right)^2 \end{bmatrix}, \quad (11)$$

where u, v, w are the components of the velocity vector in x-, y- and z- direction.

The variational of Eq. (10) with respect to C_1 and A are the continuity equation and the species equation, respectively. The variational of Eq. (10) with respect to the velocity vector $\vec{U}$ is:

$$\mu\nabla^2\vec{U} + \frac{\rho}{2C_{\Phi}}A\nabla Y + \frac{1}{2C_{\Phi}}\nabla C_1 = 0. \quad (12)$$

The variational of Eq. (10) with respect to the species concentration Y is:

$$-\rho\vec{U}\cdot\nabla A = \rho D\nabla\cdot(\nabla A) - 2\rho D\nabla\cdot(\nabla Y). \quad (13)$$

The boundary condition of the variable A on the catalyst surface is:

$$A_{\mathrm{flux}} = r + \frac{Ar}{Y^{-1}} - \frac{K\rho Ar}{(1+K\rho Y)}. \quad (14)$$

where A_{flux} is the flux at the catalyst surface of the variable A.

There are four unknown variables and four governing equations as shown in Eqs. (1), (3), (12) and (13), so the unknown variables can be solved for a given set of boundary conditions. Meanwhile, the air flow must also meet the momentum equation. Combining Eqs. (2) and (12) gives the follow relations:

$$C_1 = -2C_{\Phi}P, \quad (15)$$

$$\vec{F} = \frac{\rho}{2C_{\Phi}}A\nabla Y + \rho\vec{U}\cdot\nabla\vec{U}. \quad (16)$$

Thus, the momentum equation can be rewritten as:

$$\rho\vec{U}\cdot\nabla\vec{U} = -\nabla P + \nabla\cdot(\mu\nabla\vec{U}) + \left(\frac{\rho}{2C_{\Phi}}A\nabla Y + \rho\vec{U}\cdot\nabla\vec{U}\right). \quad (17)$$

As shown in Eq. (17), the additional volume force, F, optimizes the velocity field, resulting in the maximum convective mass transfer rate. The momentum equation with this additional volume force is referred to as the convective heat transfer field synergy equation. For a given set of boundary conditions, the optimal velocity field, which has a larger mass transfer rate than any other field flow, can be obtained by solving this field synergy equation. Furthermore, various values of the parameter, C_{Φ}, in the field synergy equation will produce different optimal velocity fields for various viscous dissipations.

4. Application of the convective mass transfer field synergy equation in plate type reactors

The convective mass transfer analysis for plate type photocatalytic oxidation reactors, which are commonly used in air purification systems, is a classical problem with wide engineering application. Thus, a plate type reactor with 25.4 mm wide, 2.7 mm in high and 76.2 mm long, as shown in Fig. 2, will be used to illustrate the applicability of the convective mass transfer filed synergy equation. The upper surface is a UV lamp, which emits ultraviolet photos. The lower surface was coated with photocatalytic material. The value of the reaction constant, k, is 1.41×10^{-6} mol $\mathrm{m^{-2}\,s^{-1}}$, and the value of the Langmuir adsorption equilibrium constant, K, is 0.93 $\mathrm{m^3\,mg^{-1}}$. The air flow is assumed to be fully developed at the air inlet with the Reynolds number of 175, while the mass friction of all the inlet air is 1.56×10^{-6}. All the boundary conditions are the same as illustrated in the following experimental analysis.

The CFD program, FLUENT 6.0, was used to solve the field synergy equations as well as the corresponding boundary conditions. The user defined scalar (UDS) in FLUENT 6.0 was used for solving Eq. (14), which was solved synchronously with the continuity equation, convective mass

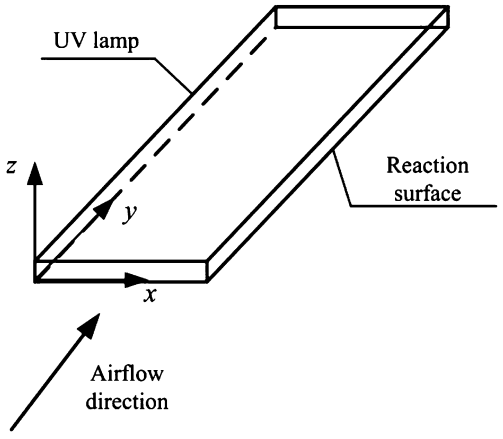

Fig. 2. Schematic of the plate type reactor.

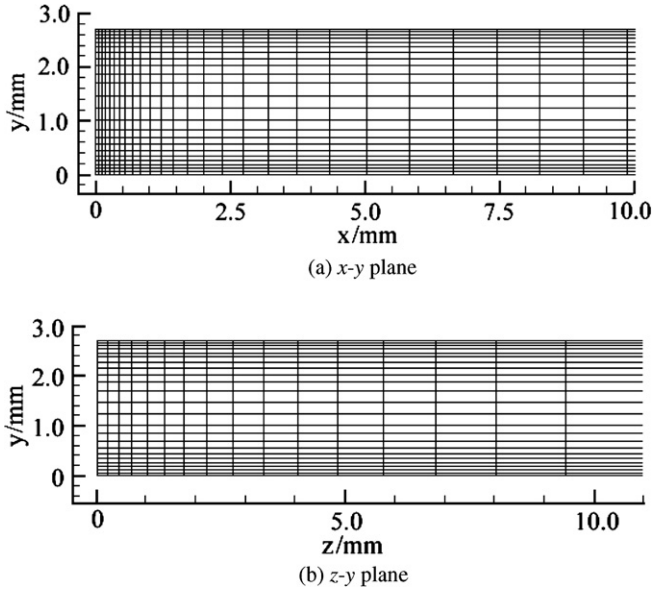

Fig. 3. Computation meshes of the plate type reactor.

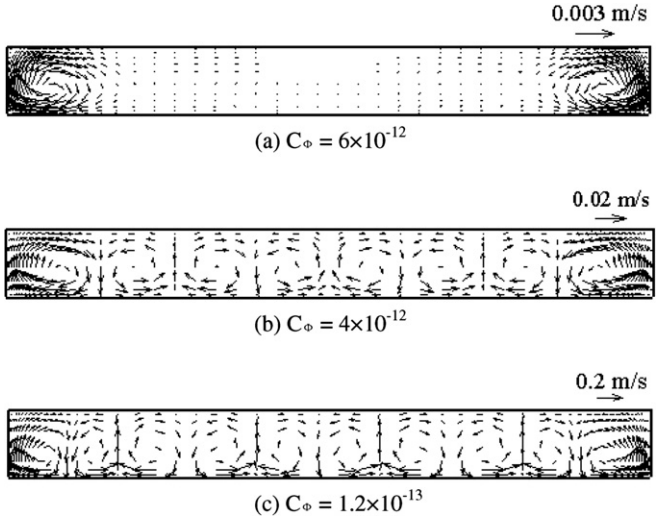

Fig. 4. Cross-section flow fields in plate type reactors for various C_Φ.

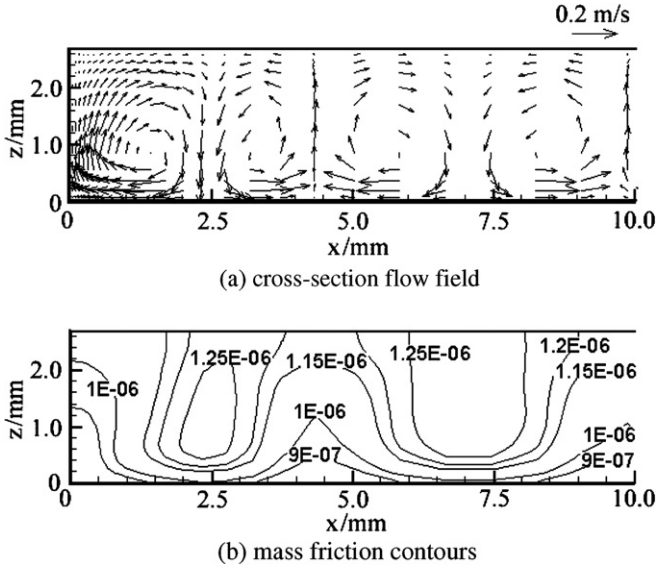

Fig. 5. Optimized results near the left wall in the section of $y = 15$ mm for $C_\Phi = 1.2 \times 10^{-13}$.

transfer field synergy equation and species equation. The user defined function (UDF) is used for adding the additional volume force in the convective mass transfer equation. The velocity and pressure were linked using the SIMPLEC algorithm with the convection and diffusion terms discretized using the QUICK format. A mesh, $60 \times 25 \times 40$, is chosen as the main computation mesh as shown in Fig. 3. The mesh is more condense in the near wall regions and near the air inlet, where more steep velocity gradient is expected.

For the original results before optimization, the velocity vectors and the contaminant concentration gradients are nearly perpendicular to each other, leading to a small scalar product between the velocity vector and the concentration gradient, so the field synergy degree as shown in Eq. (8) is relatively poor, resulting in a low mass transfer rate. In the computational domain, the viscous dissipation is 5.35×10^{-5} W, the mass transfer rate is 2.44×10^{-11} kg s^{-1} and the contaminant removal effectiveness is 40.9%.

For a given C_Φ, an optimal flow field can be obtained by numerically solving the field synergy equation as shown in Eq. (17), and then the viscous dissipation and mass transfer rate can be calculated. Meanwhile, by solving the field synergy equation with different constant, C_Φ, different optimal flow patterns for various viscous dissipations can be obtained. Fig. 4a–c are the optimized numerical results of the cross-sectional flow in the section of $y = 15$ mm for the cases of $C_\Phi = 6 \times 10^{-12}$, 4×10^{-12} and 1.2×10^{-13}. With decreasing the value of C_Φ, the strength of the longitudinal vortexes increased and the number of longitudinal vortexes occurring in the cross-section are 2, 8 and 10, respectively. The optimized cross-sectional flow field and the temperature distribution near the left wall in the section of $y = 15$ mm for $C_\Phi = 1.2 \times 10^{-13}$ are shown in Fig. 5a and b. In some part of the vortex, the fluid flows towards the contaminant surface, the included angle between the velocity vector and the concentration gradient is decreased, so the convective mass transfer field synergy is improved in this area. In the other part of the vortex, the fluid flows away from the contaminant surface, the included angle between the velocity vector and the concentration gradient is increased, so the field synergy is reduced in this area. However, the magnitude of the contaminant concentration gradient in the area of fluid flowing towards the contaminant surface is larger than in the area of fluid flowing away from the contaminant surface. So the overall field synergy is improved and the convective mass transfer is augmented. For the case of $C_\Phi = 1.2 \times 10^{-13}$, the viscous dissipation is 6.22×10^{-5} W, the mass transfer rate is

3.04×10^{-11} kg s^{-1} and the contaminant removal effectiveness is 51.1%. Compared with the original results in the smooth plate reactor before optimization, the flow viscous dissipation is increased by 16%. The mass transfer rate and the contaminant removal effectiveness are increased by 25%.

Another more condense mesh, $120 \times 40 \times 80$, is chosen to validate the numerical results are grid-independent. For the original results before optimization, the viscous dissipation is 5.35×10^{-5} W and the mass transfer rate is 2.44×10^{-11} kg s^{-1}. For the optimized results of $C_\Phi = 1.2 \times 10^{-13}$, the viscous dissipation is 6.25×10^{-5} W and the mass transfer rate is 3.05×10^{-11} kg s^{-1}. Compared with the results calculated by the original mesh, the error is small, so the numerical solutions are grid-independent.

5. Practical engineering application

The numerical analysis shows that generating multiple longitudinal vortex flow can enhance laminar mass transfer in the plate type reactor. Therefore, some certain engineering techniques, such as internal fins, can be introduced to obtain the desired velocity field to enhance the mass transfer. With the guide of the field synergy analysis for laminar mass transfer in the plate type reactor, a novel enhanced internally finned plate, discrete double-inclined ribs plate, was developed as shown in Fig. 6. Considering the limitation of manufacture, there are two pairs of double-inclined ribs perpendicular to the primary flow direction, while there are 9 ribs along the primary flow direction. The rib length in primary flow direction is 3.6 mm with the inclined angle of 45°and the rib height is 0.5 mm.

The experiments (Fig. 7) were performed to clarify the convective mass transfer characteristics the discrete double-inclined ribs plate reactor. One piece of photocatalyst-coated plate (25.4 mm wide and 76.2 mm long) was placed in the reactor, while the other same-size plate without photocatalyst was placed before the coated plate to make the reaction part in the fully developed laminar flow region. For comparison, there were two types of plates: one was the smooth plate, and the other was discrete double-inclined ribs plate. Air entered the channel from the left and exited on the right with the Reynolds number of 175.

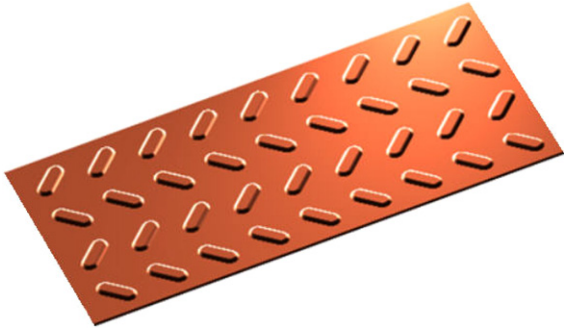

Fig. 6. Photo of the discrete double-inclined ribs plate.

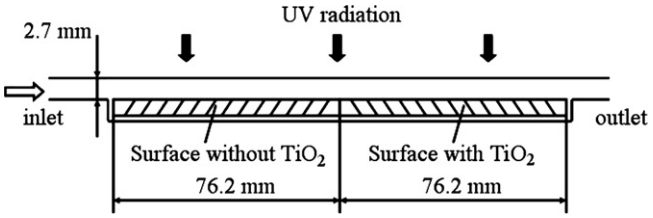

Fig. 7. Schematic of the experimental reactor.

The other boundary conditions were the same as illustrated in the numerical simulation.

The concentration of formaldehyde at the inlet and outlet of the smooth plate reactor is shown in Fig. 8. From 25 min to 55 min, the average inlet and outlet concentration of formaldehyde are 1.3 ppm and 0.77 ppm, respectively. Thus, the convective mass transfer rate is 2.5×10^{-11} kg s^{-1}, and the contaminant removal effectiveness is 41%. The concentration of formaldehyde at the inlet and outlet of the discrete double-inclined ribs plate reactor is shown in Fig. 9. From 10 min to 18 min, the average inlet

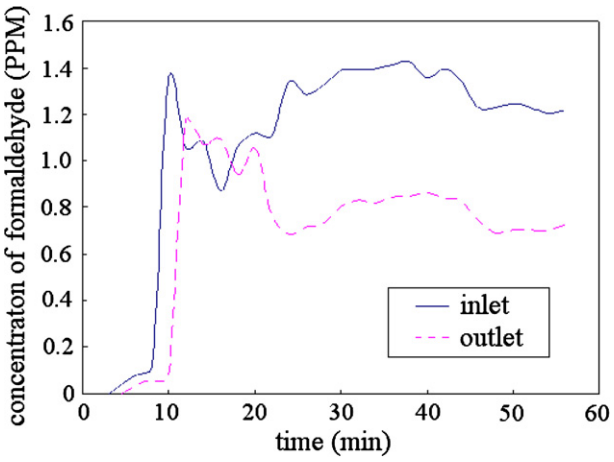

Fig. 8. Concentration of formaldehyde at the inlet and outlet of the smooth plate reactor.

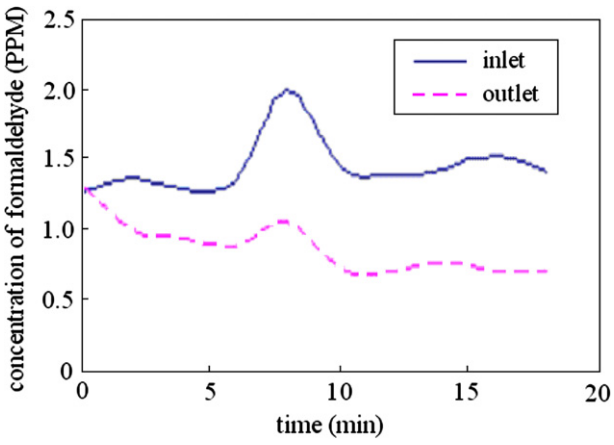

Fig. 9. Concentration of formaldehyde at the inlet and outlet of the discrete double-inclined plate reactor.

Fig. 10. Periodic segment of the discrete double-inclined plate reactor.

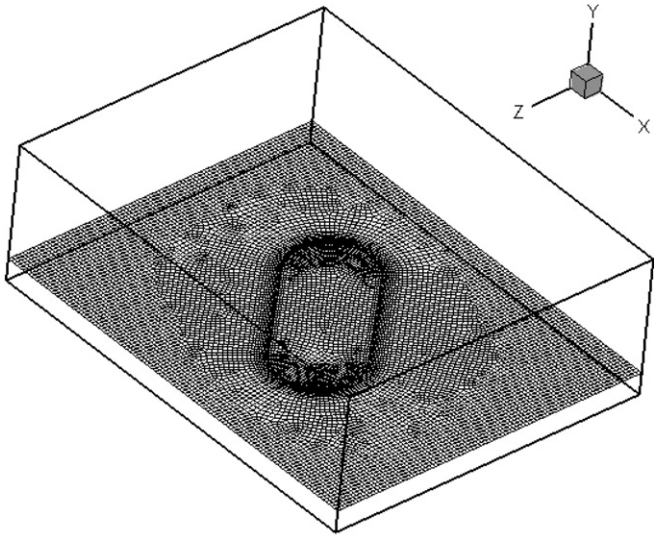

(a) *x*-*z* plane

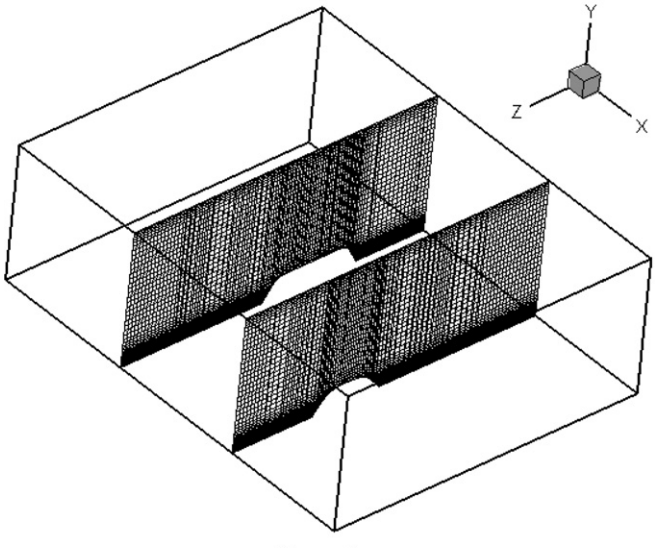

(b) *y*-*z* plane

Fig. 11. Grid distribution of the discrete double-inclined plate reactor.

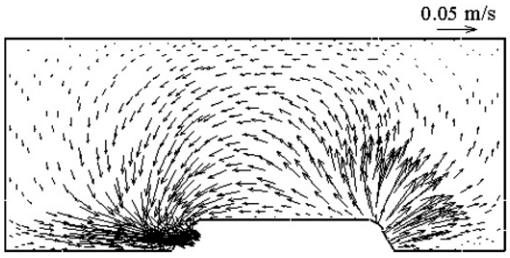

Fig. 12. Cross-sectional flow fields nearby an internal fin in the internally fined plate reactor.

and outlet concentration of formaldehyde are 1.4 ppm and 0.7 ppm , respectively. Thus, the convective mass transfer rate is 3.1×10^{-11} kg s^{-1}, and the contaminant removal effectiveness is 50%. Compared with the smooth plate reactor, the mass transfer rate and the contaminant removal effectiveness are increased by 24% and 22%, respectively.

A numerical simulation was carried out to obtain the flow pattern in the discrete double-inclined plate reactor. A repeated segment with four inclined ribs was chosen to be simulated as shown in Fig. 10. The flow and mass transfer were assumed periodically fully developed due to the long tested plate. For saving time and memory, only one fourth of the periodic segment was mashed and simulated due to the symmetry. Fig. 11 shows the grid distribution. A structural grid with hexahedral elements was generated. The grid near the walls is intensified and the total element of the grid is 450,000.

Because of the complex flow inside the discrete double-inclined ribs pate reactor, turbulence may originate even at low Reynolds number especially near the rib region. For low Reynolds number heat transfer, $Re < 1000$, in the alternate elliptical axis tube, Meng [23] showed that the numerical results predicted by the RNG k–ε model were more accurate than that by the laminar model. Thus, the RNG k–ε model was utilized in this paper. Fig. 12 depicts the numerical cross-section flow field in the domain nearby an internal fin. A longitudinal vortex is induced by the discrete double-inclined rib on the internal wall, which is similar to the optimal flow field obtained by solving the field synergy equation. The longitudinal vortex improves the field synergy between the velocity and contaminant concentration gradient fields and enhances the convective mass transfer. There are also several longitudinal vortexes nearby the other ribs for symmetry.

In a word, the solution of the field synergy equation gives the optimal velocity field to guide the photocatalytic oxidation reactor design and maximize the contaminant removal effectiveness finally.

6. Conclusions

A convective mass transfer field synergy equation with a specific boundary condition developed based on the extremum principle of mass transfer potential capacity dissipation was solved to predict the optimum convective mass

transfer flow field in photocatalytic oxidation reactors. This field synergy equation is similar to the momentum equation with a special additional volume force, which can optimize the velocity field to improve the field synergy between the velocity and species concentration gradient fields and enhance convective mass transfer finally. Variation of the additional volume force term in the field synergy equation leads to different optimal velocity fields for different viscous dissipations.

The solution of the field synergy equation gives that the optimal flow field in the plate type reactor, which can enhance laminar mass transfer effectively, is the multi-longitudinal vortex flow. The predicted optimal flow pattern in the plate type reactor was then used to design the discrete double-inclined ribs plate in actual applications to generate the desired multi-longitudinal vortex flow close to the optimal one. The experimental result shows that the contaminant removal effectiveness for this specific internally finned plate is increased by 21% compared to the smooth plate reactor.

Acknowledgements

This work was supported by National Nature Science Foundation of China (Grant No. 50276033, 50436040). Thanks for Mr. Xu, Q. J., Dept. of Building Science, Architecture School, Tsinghua University in the experiments.

References

[1] J. Sundell, What we know, and don't know about sick building syndrome, ASHRAE J. 38 (1996) 51–57.
[2] P. Wargocki, D.P. Wyon, Y.K. Baik, G. Clausen, P.O. Fanger, Perceived air quality, sick building syndrome (SBS) and productivity in an office with two different pollution loads, Indoor Air 9 (1999) 165–179.
[3] U.S. EPA. 1991. Sick building syndrome (SBS), Indoor Air Facts No. 4 (revised), U.S. Environmental Protection Agency, Washington, DC.
[4] J. Peral, D.F. Ollis, Heterogeneous photocatalytic oxidation of gas-phase organics for air purification: acetone, 1-butanol, butyraldehyde, formaldehyde, and *m*-xylene oxidation, J. Catal. 136 (1992) 554–565.
[5] T.N. Obee, R.T. Brown, TiO_2 photocatalysis for indoor air applications: effects of humidity and trace contaminant levels on the oxidation rates of formaldehyde, toluene, and 1, 3-butadiene, Environ. Sci. Technol. 29 (1995) 1223–1231.
[6] R.M. Alberici, W.E. Jardim, Photocatalytic destruction of VOCs in the gas-phase using titanium dioxide, Appl. Catal. B – Environ. 14 (1997) 55–68.
[7] W.K. Jo, J.H. Park, H.D. Chun, Photocatalytic destruction of VOCs for in-vehicle air cleaning, J. Photochem. Photobiol. A Chem. 148 (2002) 109–119.
[8] A. Vohra, D.Y. Goswami, D.A. Deshpande, S.S. Block, Enhanced photocatalytic disinfection of indoor air, Appl. Catal. 65 (2006) 57–65.
[9] D.T. Tompkins, D.T. ASHRAE Research Project 1134-RP: Evaluation of Photocatalytic Air Cleaning Capability (Final Report); ASHRAE: Atlanta, GA, 2001.
[10] R. Yang, Y.P. Zhang, Q.J. Xu, A mass transfer based method for measuring the reaction coefficients of a photocatalyst, Atmos. Environ. 41 (6) (2007) 1221–1229.
[11] Y.P. Zhang, R. Yang, Q.J. Xu, Characteristics of photocatalytic oxidation of toluene, benzene and their mixture, J. Air Waste Manage. Assoc. 57 (2007) 94–101.
[12] Y. Parent, D. Blake, B.K. Magrini, C. Lyons, C. Turchi, A. Watt, E. Wolfrum, M. Prairie, Solar photocatalytic processes for the purification of water: state of development and barriers to commercialization, Solar Energy 56 (1996) 429–437.
[13] J. Mo, Y. Zhang, R. Yang, Novel insight into VOC removal performance of photocatalytic oxidation reactors, Indoor Air 15 (2005) 291–300.
[14] Z. Zhang, W.A. Anderson, M. Moo-Young, Experimental analysis of a corrugated plate photocatalytic reactor, Chem. Eng. J. 99 (2004) 145–152.
[15] Y.P. Zhang, R. Yang, R.Y. Zhao, A model for analyzing the performance of photocatalytic air cleaner in removing volatile organic compounds, Atmos. Environ. 37 (2003) 3395–3399.
[16] Z.Y. Guo, W.Q. Tao, R.K. Shah, The field synergy (coordination) principle and its applications in enhancing single phase convective heat transfer, Int. J. Heat Mass Transfer 48 (2005) 797–1807.
[17] W.Q. Tao, Y.L. He, Q.W. Wang, Z.G. Qu, F.Q. Song, A unified analysis on enhancing single phase convective heat transfer with field synergy principle, Int. J. Heat Mass Transfer 45 (2002) 4871–4879.
[18] J.A. Meng, X.G. Liang, Z.X. Li, Field synergy optimization and enhanced heat transfer by multi-longitudinal vortices flow in tube, Int. J. Heat Mass Transfer 48 (2005) 3331–3337.
[19] Z.Y. Guo, H.Y. Zhu, X.G. Liang, Entransy—a physical quantity describing heat transfer ability, Int. J. Heat mass transfer 50 (2007) 2545–2556.
[20] Q. Chen, J.X. Ren, Z.Y. Guo, Field synergy analysis and optimization of decontamination ventilation designs, Int. J. Heat Mass Transfer 50 (2007), in press, doi:10.1016/j.ijheatmasstransfer.2007.04.004.
[21] B.A. Finlayson, The Method of Weighted Residuals and Variational Principles—with Application in Fluid Mechanics, Heat and Mass Transfer, Academic Press, New York, 1972.
[22] M. Ichiyanagi, Variational principles of irreversible processes, Phys. Rep. 243 (3) (1994) 125–182.
[23] J.A. Meng, X.G. Liang, Z.X. Li, Z.Y. Guo, Numerical study on low Reynolds number convection in alternate elliptical axis tube, J. Enhanced Heat Transfer 11 (2004) 307–313.